Paper

Soft Touch Mass-Reduced-Mode Control of Attractive Force in SLIM Vehicle Propulsion

Kinjiro Yoshida* Member
Takashi Yoshida* Student Member

Based on the decoupled-control method of attractive-normal and thrust forces, a compact combined-levitation-and-propulsion single-sided linear induction motor (SLIM) maglev vehicle system can be realized without any additional levitation magnets. In this paper, we have proposed a mass-reduced mode control of the SLIM vehicle based on its decoupled-control method and succeeded in a stable propulsion control experiment in 95%-mass-reduced mode at a minimum airgap-length of 1.7 mm limited by guide-rollers even by using a simple construction of wheel and rail system without primary suspension. The vehicle has been propelled with the minimum power for supporting the vehicle by realizing simultaneously the minimum airgap and the soft-touch, so that it has been driven with small noises and vibrations because of very soft contact. And considering the wear and the maintenance, this running method with soft-touch mass-reduced control is very useful for many practical applications.

Keywords: SLIM, combined-levitation-and-propulsion, decoupled-control, mass-reduced mode, attractive normal-force, soft touch

1. Introduction

In Maglev vehicle system, SLIM is often used to provide propulsion with additional levitation magnet [1][2]. The control of SLIM is of constant slip-frequency system to eliminate the problem of the normal force which has been pointed out as a drawback of the SLIM [2]. On the other hand, combined-levitation-and-propulsion SLIM Maglev vehicle which is used in this study is based on a unified concept of machine principle, in which combined magnetic levitation-and-propulsion using only one linear motor has been proposed as a compact system without any additional magnets for levitation [3]. Controlled-repulsive linear synchronous motor (LSM) Maglev vehicles have been designed and simulated for feasibility study [4][5]. A decoupled-control method of

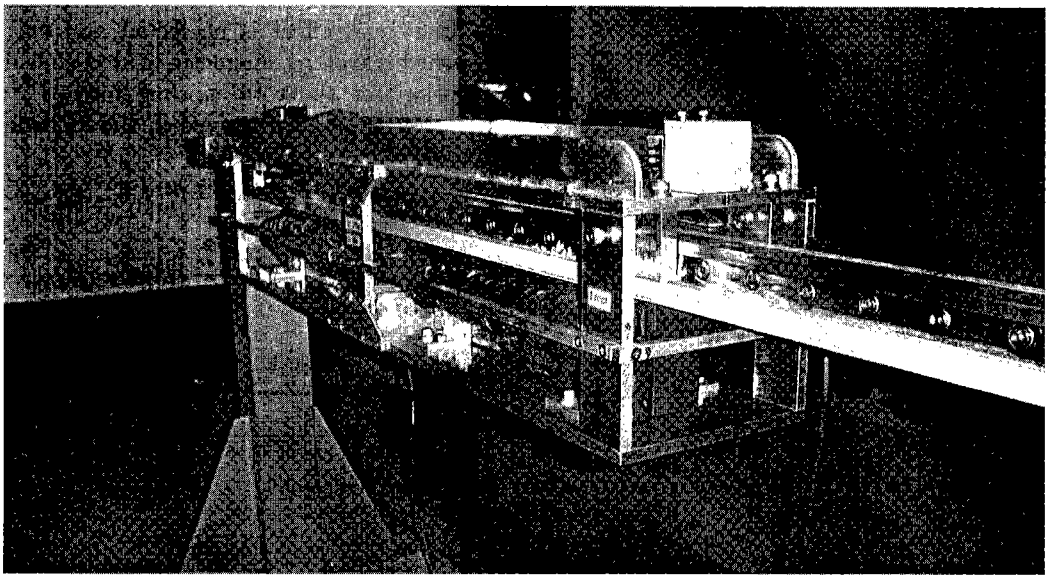

Fig. 1. SLIM experimental Maglev vehicle.

* Department of Electrical and Electronic Systems Engneering, Graduate School of Information Science and Electrical Engineering, Kyushu University
10-1 6-chome Hakozaki Higashi-ku, Fukuoka 812-8581

lift and thrust forces has been proposed and effectively used [6]. Marine express (ME) 03 has been realized successfully [7].

Controlled-attractive SLIM Maglev vehicle has been proposed and experimented based on a decoupled-control method of attractive-normal and thrust forces [8]. To realize a stable levitation and propulsion of SLIM vehicle, normal and thrust forces in a SLIM must be controlled independently [8]~[10] and the pitching motion of the vehicle must be restrained simultaneously [9] [10]. The decoupled-control method of attractive-normal and thrust forces is derived from the analytical formulas for normal and thrust forces in the SLIM with secondary back-iron. Based on this method, the attractive-normal force is used to levitate the vehicle and the thrust force to propel the vehicle without coupling between these two forces. A compact combined-levitation-and-propulsion SLIM Maglev vehicle system can be therefore realized without any additional levitation magnets and the vehicle can levitate independently of the vehicle speed.

This paper presents that a mass-reduced mode control of combined-levitation-and-propulsion SLIM maglev vehicle can be realized based on the decoupled-control of normal and thrust forces in SLIM and the vehicle has been levitated stably in 95%-mass-reduced mode at a minimum airgap of 1.7 mm and has been suspended with guide-rollers contacting very softly with the guideway. Furthermore we compared the mass-reduced mode experiment with completely-levitated experiment and clear the usefulness of mass-reduced mode.

2. SLIM Maglev Vehicle and Mass-reduced Mode

Figure 1 shows a SLIM experimental Maglev vehicle. The vehicle is designed and manufactured in a mono rail type, which runs along the 3 m long linear motor guideway of reaction plate in our Laboratory. The vehicle with two independent armatures mounted straight-line at the front and the rear on board is 96 cm in length and 42.25 kg in weight, and the guideway consists of aluminum reaction plate and back-iron. The vehicle is levitated and propelled by only a pair of armature and secondary conductor. The attractive-normal force is used to levitate the vehicle and the thrust force to propel the vehicle without coupling between these two forces.

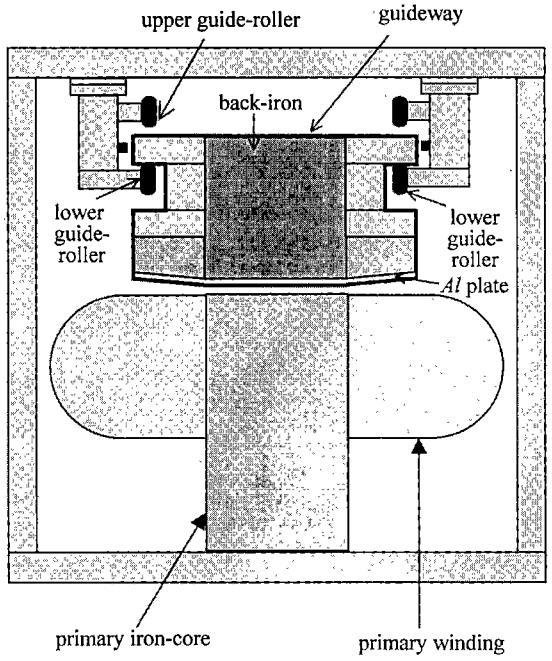

Fig. 2. Transverse cross-section of SLIM experimental Maglev vehicle.

Figure 2 shows a cross-section of the SLIM experimental Maglev vehicle. It is 19 cm in height and width. In Fig. 2, when upper guide-rollers contact with the guideway, the airgap-length δ is 6.0 mm. When lower guide-rollers contact with the guideway, the airgap-lengths at the front and rear are 1.6 mm and 1.8 mm respectively. Therefore, the possible pitching-angle limited by guide rollers is about -0.263 deg $\sim$ 0.251 deg. In mass-reduced mode, the vehicle is levitated but limited by lower guide-rollers at a minimum airgap as shown in Fig. 2. By using mass-reduced control mode the vehicle can be propelled contacting very softly the lower guide-rollers with the guideway. In this system, levitation and pitching motion of the vehicle are controlled independently. Contacting simultaneously the front and rear lower guide-rollers on the guideway, we select 1.7 mm for the demand airgap-lengths, which is the average value of the front and rear airgap-length of 1.6 mm and 1.8 mm above mentioned.

3. Decoupled-control of Normal and Thrust Forces and Mass-reduced Mode

Decoupled-control method of normal and thrust forces is derived from the analytical formulas for normal and thrust forces in the SLIM with secondary back-iron using space harmonic analysis method [11].

In this paper, to derive an analytical formula for decoupled-control of normal and thrust forces, the short-primary end effect is neglected and only fundamental forward-travelling magnetic field is considered. The expression for the total normal force F_z and the total thrust force F_x are derived in the following forms:

$$F_z = \frac{2\mu_0 hm^2 k_{w1}^2 N_{ph}^2}{p\tau} I_1^2 (K^2 - 1) \quad \cdots\cdots\cdots\cdots (1)$$

$$F_x = \frac{4\mu_0 hm^2 k_{w1}^2 N_{ph}^2}{p\tau} I_1^2 \mathrm{Re}(-jK_H^*) \quad \cdots\cdots\cdots (2)$$

Table 1. Specifications of SLIM.

Item	Symbol	Value
Number of phase	m	3
Number of pole	p	6
Pole pitch	τ	51mm
Width of primary iron core	h	50mm
Number of slots per pole per phase	q	1
Turns per phase	N_{ph}	300
Winding coefficient	k_{w1}	1.0
Thickness of secondary back-iron	d_1	50mm
Thickness of aluminum secondary	d_2	2.0mm

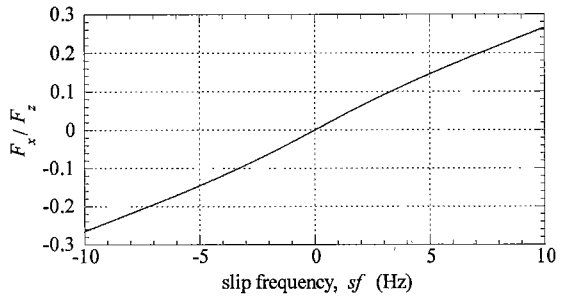

Fig. 3. F_x/F_z for sf in mass reduced mode at the airgap-length of 1.7 mm.

where μ_0 is the permeability of air, I_1 the effective value of armature current. And K, K_H^* are described as a function of slip-frequency sf and airgap-length δ. The specifications of SLIM are shown in Table 1.

Considering F_x/F_z as a parameter in the analysis of a SLIM, it can be derived as a function of slip-frequency sf as follows:

$$\frac{F_x}{F_z} = 2\mathrm{Re}\left(\frac{-jK_H^*}{K^2-1}\right) = f(sf) \cdots\cdots\cdots\cdots (3)$$

Figure 3 shows the F_x/F_z for the slip-frequency sf of the SLIM at the airgap-length of 1.7 mm. Figure 3 means that in mass-reduced mode a slip-frequency sf can be determined uniquely from one variable F_x/F_z. It is an important characteristic to realize a mass-reduced mode control. In addition, it is clear that a standstill levitation with $F_x = 0$ can be also realized by feeding a direct-current ($f = 0$) into primary-windings. Because there is back-iron in the secondary, a large attractive normal-force is obtained to suspend the vehicle with short-primary underneath.

4. Mass-reduced Mode Control

Figure 4 shows the block diagram of the mass-reduced mode control systems for the SLIM experimental Maglev vehicle. According to the optimal robust servo control theory, to follow quickly the demand patterns of vehicle position x_{20}, speed v_{x20} and levitation height z_0 and to restrain the pitching motion, command normal force F_z^*, thrust force F_x^* and pitching torque T_ϕ^* are determined as follows:

$$F_x^* = k_{x\mathrm{P}}(x_{20}-x_2) + k_{x\mathrm{D}}(v_{x20}-v_{x2}) + k_{x\mathrm{I}}\int(x_{20}-x_2)dt + M\dot{v}_{x20} \cdots\cdots (4)$$

$$F_z^* = k_{z\mathrm{P}}(z_0-z) + k_{z\mathrm{D}}(\dot{z}_0-\dot{z}) + k_{z\mathrm{I}}\int(z_0-z)dt + M\dot{z}_0 + Mg + \varepsilon Mg \cdots\cdots (5)$$

$$T_\phi^* = -k_{\phi\mathrm{P}}\phi - k_{\phi\mathrm{D}}\dot{\phi} - k_{\phi\mathrm{I}}\int\phi dt \cdots\cdots (6)$$

Where x_2, v_{x2}, z, $\dot{z}$, ϕ, and $\dot{\phi}$ are the measured vehicle position, vehicle speed, levitation height and speed in the z-direction, pitching-angle and pitching-angle speed, respectively, $k_{x\mathrm{P}}$, $k_{x\mathrm{D}}$ and $k_{x\mathrm{I}}$ are the feedback gains for propulsion control, $k_{z\mathrm{P}}$, $k_{z\mathrm{D}}$ and $k_{z\mathrm{I}}$ are the feedback gains for levitation control, $k_{\phi\mathrm{P}}$, $k_{\phi\mathrm{D}}$ and $k_{\phi\mathrm{I}}$ are the feedback gains for pitching control. εMg is the load against the guideway. Hence the vehicle is driven in $(1-\varepsilon)\times 100\%$-mass-reduced mode.

Then, from the command normal force F_z^*, thrust force F_x^* and pitching torque T_ϕ^*, command normal forces $F_{z\mathrm{F}}^*$, $F_{z\mathrm{R}}^*$ and the command thrust forces $F_{x\mathrm{F}}^*$, $F_{x\mathrm{R}}^*$ of the front and rear SLIM are calculated according to equations (7)~(10).

$$F_x^* = F_{x\mathrm{F}}^* + F_{x\mathrm{R}}^* \cdots\cdots (7)$$

$$F_z^* = F_{z\mathrm{F}}^* + F_{z\mathrm{R}}^* \cdots\cdots (8)$$

$$T_\phi^* = F_{z\mathrm{F}}^*(-d\sin\phi - l\cos\phi) + F_{x\mathrm{F}}^*(d\cos\phi - l\sin\phi) + F_{z\mathrm{R}}^*(-d\sin\phi + l\cos\phi) + F_{x\mathrm{R}}^*(d\cos\phi + l\sin\phi) \cdots\cdots (9)$$

$$F_{x\mathrm{F}}^* = F_{x\mathrm{R}}^* \cdots\cdots (10)$$

Command slip-frequency sf_{F}^* of the front SLIM is calculated from the normal force $F_{z\mathrm{F}}^*$ and thrust force $F_{x\mathrm{F}}^*$, which are based on Fig. 4. Then command effect value

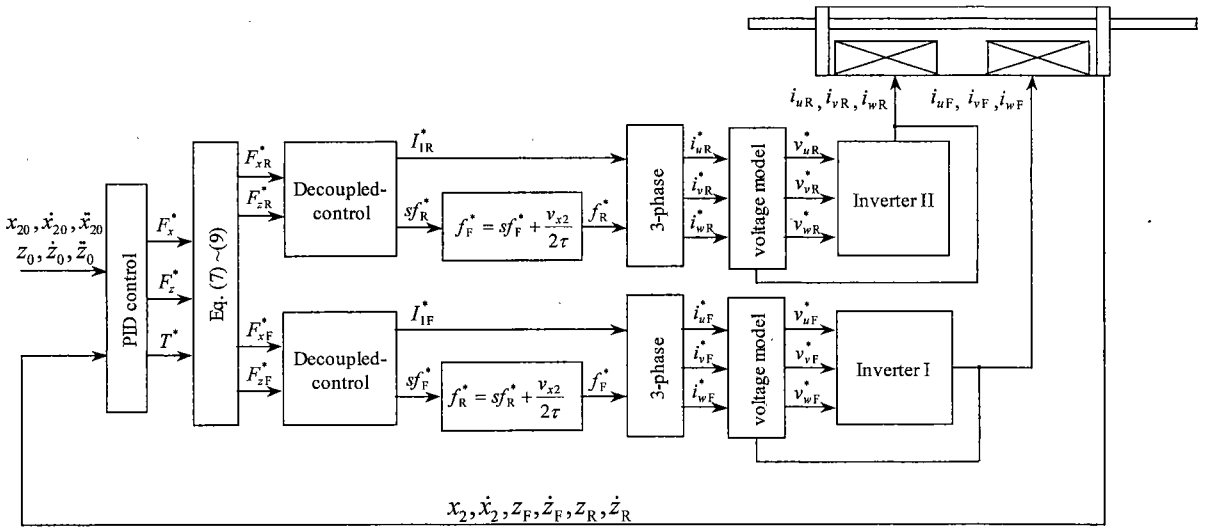

Fig. 4. Block diagram of the mass-reduced mode control systems for SLIM experimental Maglev vehicle.

of armature-current of front SLIM $I^*_{1\mathrm{F}}$ can be calculated from $F^*_{z\mathrm{F}}$, sf^*_{F} and demand airgap length δ_{F} as follows [8] [9]:

$$I^*_{1\mathrm{F}} = f_{I_1}(F^*_{z\mathrm{F}}, sf^*_{\mathrm{F}}, \delta_{\mathrm{F}}) \quad \cdots\cdots\cdots\cdots\cdots\cdots (11)$$

In addition, command frequency f^*_{F} can be also determined from considering sf^*_{F} together with the vehicle speed v_{x2}. Similarly, sf^*_{R}, $I^*_{1\mathrm{R}}$, f^*_{R} are determined. In brief, for arbitrary F^*_x, F^*_z and T^*_ϕ, $I^*_{1\mathrm{F}}$, f^*_{F}, $I^*_{1\mathrm{R}}$ and f^*_{R} can be determined uniquely and the vehicle can be levitated by normal force and propelled by thrust force in the SLIM.

Figure 5 shows a SLIM experimental system. The calculation of motion control is done by the Main PC. Its sampling time is 1.0 ms. The calculated data of command values of current $i^*_{u\mathrm{F}}$, $i^*_{v\mathrm{F}}$, $i^*_{u\mathrm{R}}$, $i^*_{v\mathrm{R}}$ are sent to the DSP. The calculation of control current whose sampling time is 0.1 ms is done by the DSP. The calculated data of command values of voltage $v^*_{u\mathrm{F}}$, $v^*_{v\mathrm{F}}$, $v^*_{w\mathrm{F}}$, $v^*_{u\mathrm{R}}$, $v^*_{v\mathrm{R}}$, $v^*_{w\mathrm{R}}$ are sent to two PWM modulations. A laser sensor is used as the gap sensor and a target sensor is used as the position sensor. A carrier frequency of the inverter is 10 kHz and electromagnetic noise is very small.

5. Experiment of Combined-levitation-propulsion SLIM Maglev Vehicle in 95%-mass-reduced Mode

5.1 95%-mass-reduced mode Considering the wear and the maintenance, the smaller the load against the guideway εMg is, the better combined-levitation-propulsion SLIM Maglev system is. But εMg is determined by the performance of the control system and the mechanical accuracy. For example, this experimental system was designed in the limit of 2.0~6.0 mm in airgap-length, but actually the limitations of front and rear airgap-lengths are 1.6~6.0 mm and 1.8~6.0 mm respectively. This is because of the mechanical accuracy of the guide-rollers. In this experiment, ε was 0.05. So the vehicle was driven in 95%-mass-reduced mode and the load of one lower guide-roller is about 5.2N and it is very small compared with the weight of the vehicle.

Table 2. Comparison of standstill-levitation loss between mass-reduced mode and completely-levitated experiments.

Experiments	Standstill-levitation period of 0.0-3.5s and 11.5-15.0s in the 95%-mass-reduced mode experiment	Completely-levitated experiment
Average loss during steady state	400.1W (2.0-3.5s and 11.5-13.0s)	939.0W (2.0-5.0s)

5.2 Experimental results In the experiment, an initial airgap-length is 6 mm with the upper guide-rollers contacting on the guideway. The vehicle is first levitated upward from airgap-length 6 mm to the demand airgap-length 1.7 mm at standstill, then shuttled along the guideway of 1.8 m between two pillars at a maximum speed of 0.72 m/s and at a maximum acceleration of 1.44 m/s^2. After that, the vehicle is controlled to land at standstill.

Figure 6 gives the experimental results of combined-levitation-propulsion SLIM vehicle in 95%-mass-reduced mode. As shown in Fig. 6(a) and (b) vehicle position x_2 and speed v_{x2} were controlled to follow the demand pattern x_{20} and v_{x20} very well. Figure 6(c) and (d) show the levitation height at the center of the vehicle z_{C}, the levitation heights at the front and rear z_{F}, z_{R}. These were also controlled to follow the demand pattern z_0 very well. Figure 6(e) and (f) show the airgap-lengths at the front and rear δ_{F}, δ_{R} and the pitching angle ϕ. In Fig. 6(e), the vehicle was propelled with a small average difference of about 0.2 mm between δ_{F} and δ_{R} on which small deviations are superposed. As shown in Fig. 6(f), with inclining backward with an offset of about 0.03 deg due to installation irregularity of the guide-rollers, a pitching motion is thus caused which fluctuates within about $\pm$0.01 deg due to contact irregularity between lower guide-roller and its guideway. Figure 6(g), (h) and (i) show the command thrust forces of the front and the rear SLIM $F^*_{x\mathrm{F}}$, $F^*_{x\mathrm{R}}$, the com-

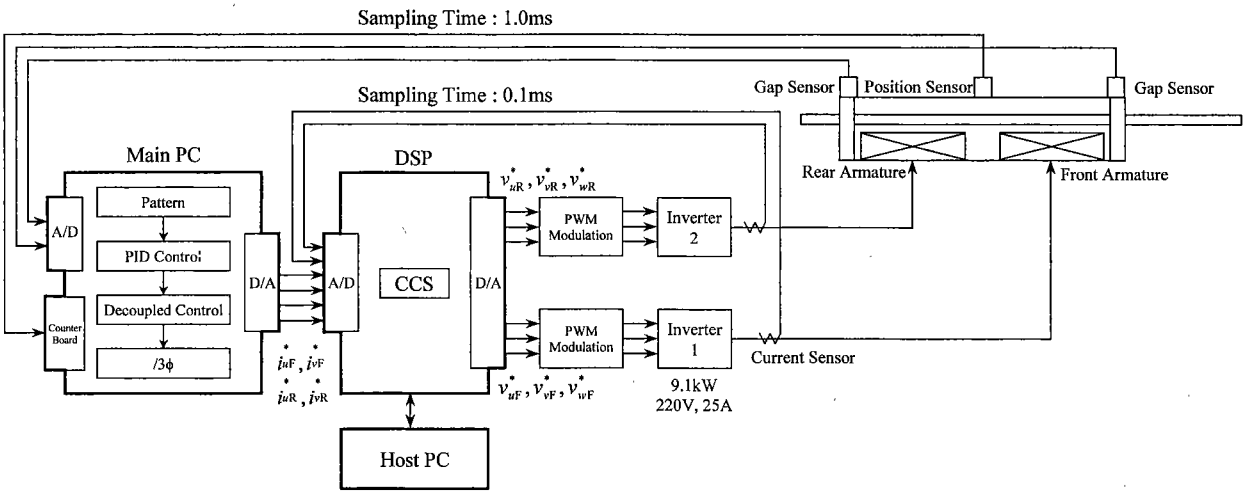

Fig. 5. SLIM experimental system.

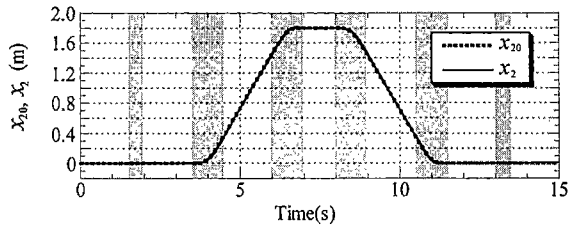

(a) Demand and measured vehicle positions

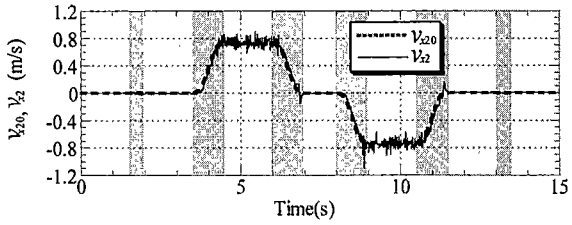

(b) Demand and measured vehicle speeds

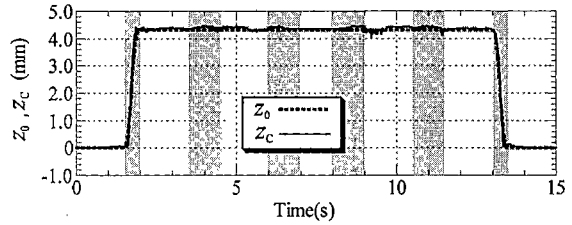

(c) Demand and measured levitation heights at center

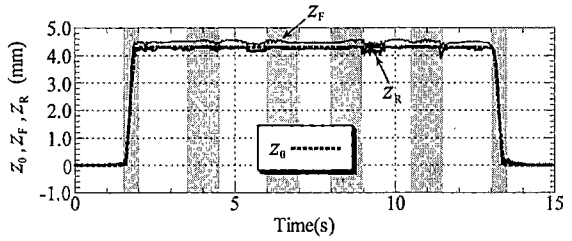

(d) Demand and measured levitation heights at front and rear

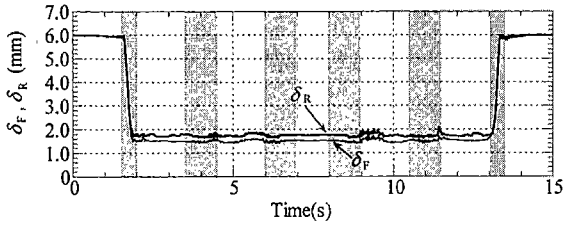

(e) Measured airgap-lengths at front and rear

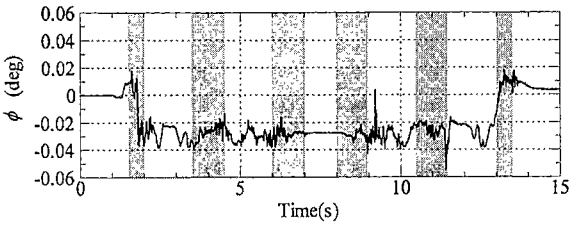

(f) Measured pitching angle

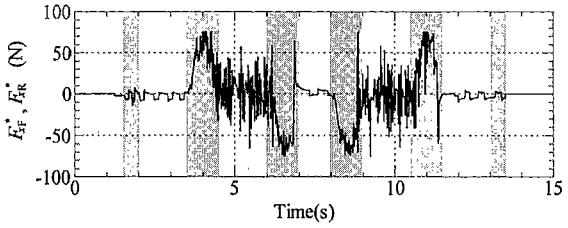

(g) Command thrust forces of front and rear SLIM

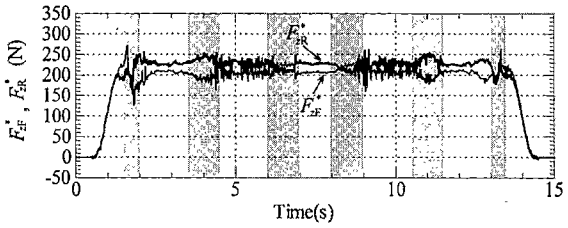

(h) Command normal forces of front and rear SLIM

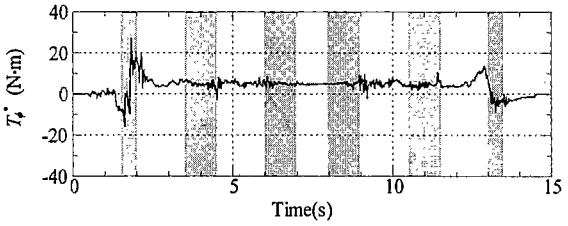

(i) Command pitching torque

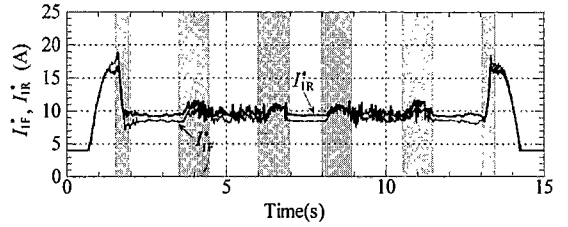

(j) Command effective values of primary current of front and rear armature

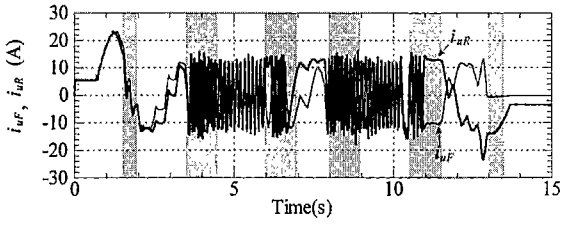

(k) Measured instantaneous values of u-phase current of front and rear armature

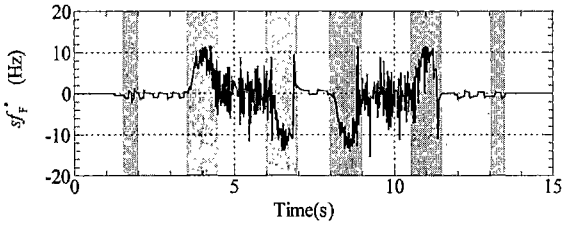

(l) Command slip-frequency of front SLIM

Fig. 6. Results of levitation-propulsion control of SLIM experimental vehicle in 95%-mass-reduced mode.

mand normal forces of the front and the rear SLIM F_{zF}^*, F_{zR}^* and the command pitching torque T_ϕ^*. Figure 6(j), (k) and (l) show the command effective values of primary-current of the front and rear armatures I_{1F}^*,

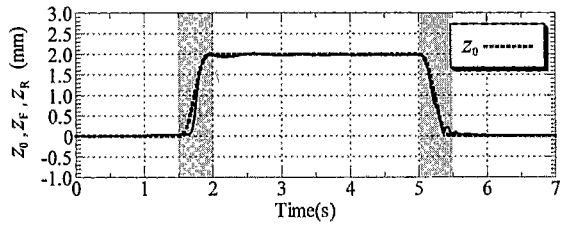

(a) Demand and measured levitation heights at front and rear

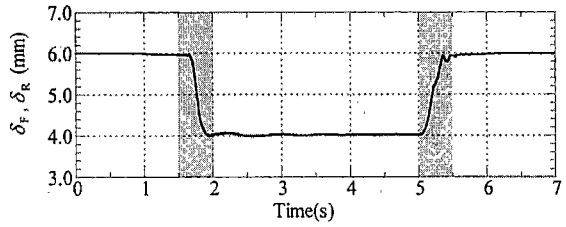

(b) Measured airgap-lengths at front and rear

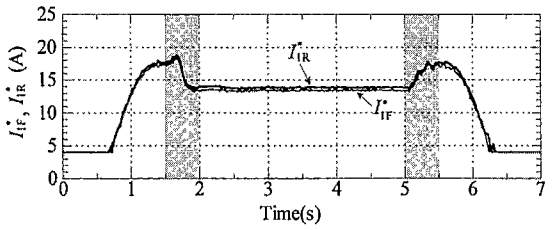

(c) Command effective values of primary current of front and rear armature

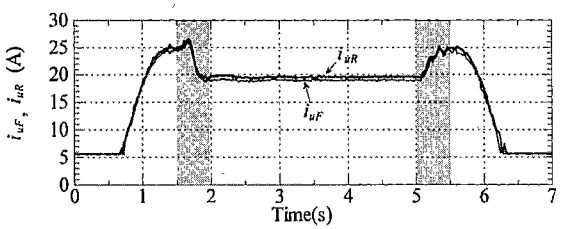

(d) Measured instantaneous values of u-phase current of front and rear armature

Fig. 7. Results of levitation control of SLIM experimental Maglev vehicle at the normal airgap-length of 4 mm at standstill.

I_{1R}^*, measured instantaneous values of u-phase current of the front and rear armatures i_{uF}, i_{uR}, command slip-frequency of the front SLIM sf_F^*, respectively. During a standstill-levitation period, I_{1F}^* and I_{1R}^* were up to a maximum values of about 19 ampere and 17 ampere to levitate the vehicle from a rest state. As the airgap-length became small, I_{1F}^* and I_{1R}^* were reduced. And I_{1F}^* and I_{1R}^* were the minimum values of about 9 ampere and 8 ampere when corresponding airgap-lengths at the front and the rear were the minimum values of 1.6 mm and 1.8 mm with the lower guide-rollers contacted with the guideway.

5.3 Comparison of Standstill-levitation Between Mass-Reduced Mode and Completely-Levitated Experiments Figure 7 shows the experimental results of levitation control of SLIM experimental Maglev vehicle at the normal airgap-length of 4 mm at standstill. Figure 7(a) and (b) show the levitation heights at the front z_F and the rear z_R and the airgap-lengths at the front and rear δ_F, δ_R. Figure 7(c) and (d) show the command effective values of primary-current of the front and rear armatures I_{1F}^*, I_{1R}^* and measured instantaneous values of u-phase current of the front and rear armatures i_{uF}, i_{uR} respectively. This experiment corresponds to the standstill-levitation period of 0.0–3.5 s and 11.5–15.0 s in the experiment of combined-levitation-propulsion SLIM Maglev vehicle in 95%-mass-reduced mode. Table 2 shows the comparison of standstill-levitation loss between mass-reduced mode and completely levitated experiments. The average loss during steady state in the 95%-mass-reduced mode experiment was 400.1 W and the average loss during steady state in the completely-levitated experiment was 939.0 W. From Table 2, it is found that the average loss during steady state in the 95%-mass-reduced mode experiment decreased by 57.4% compared with the average loss during steady state in the completely-levitated experiment. In the completely-levitated experiment with very small airgap-length of 1.7 mm, it is extremely difficult to control stably the vehicle for very complex fluctuations caused due to the elastic guideway of conventional structure and irregularities of installation and guideway. On the other hand, it is easily possible to control the vehicle even at the demand airgap-length of 1.7 mm in the mass-reduced-mode experiment because the propelling vehicle is supported mechanically but very softly by means of the relatively small guide-rollers. The average loss during steady state in the 95%-mass-reduced mode experiment is decreased considerably compared with that in the completely-levitated experiment, because of the large difference in the demand airgap-length between the two experiments. In the principle of mass-reduced-mode experiment with attractive force, the loss increases a little by reaction force through the guide-rollers between the vehicle and guideway. But in this experiment ε was 0.05 and the reaction force was very small.

6. Conclusions

In this paper, we proposed the mass-reduced mode control of combined-levitation-and-propulsion SLIM vehicle based on the decoupled-control of attractive normal and thrust forces in SLIM. Propulsion control experiment in 95%-mass-reduced mode of the SLIM vehicle has been carried out contacting very softly guide-rollers with guideway. The following results have been obtained:

(1) 95%-mass-reduced mode has been carried out stably even by using a simple construction of wheel and rail system without primary suspension.

(2) The vehicle has been driven with minimization of input power for supporting the vehicle by realizing simultaneously the minimum airgap limited by guide-rollers and the soft-touch.

(3) The vehicle has been driven with small noises and vibrations because of very soft contact. And considering the wear and maintenance, this running method with

soft-touch mass-reduced control is very useful for many practical applications.

(Manuscript received May 23, 2002,
revised November 29, 2002)

References

(1) K.R. Davey: "Transverse Flux Linear Induction Motors Applied to Magnetic Suspension System", *Proc. of 6th ISMST*, Vol.1, pp.349–353 (2001-10)

(2) S. Suzuki, M. Kawashima, Y. Hosoda, and T. Tanida: "HSST-03 System", *IEEE Trans. on Magn.*, **MAG-20**, No.5, pp.1675–1677 (1984-9)

(3) K. Yoshida: "Magnetic Levitation and Linear Motor, Science of Machine", **42**, No.4, pp.468–474 (1990)

(4) K. Yoshida and S. Nagao: "Levitation and Propulsion Control and Simulation of Superconducting LSM Maglev Vehicle", *Report of LD-90-63 of the Joint Studying Committee on Magnetics and Linear Drives*, pp.39–48 (1990)

(5) K. Yoshida and S. Nagao: "Levitation and Propulsion Control Simulation of Regardless-of-speed Superconducting LSM Repulsive Maglev Vehicle", *Proc. of the 3rd Electromagnetics Symposium*, pp.201–206 (1991)

(6) K. Yoshida, H. Takami, and L. Shi: "Decoupled-Control of Levitation and Propulsion in Underwater LM car ME02", *the Journal of Mathematics and Computers in Simulation*, **46**, pp.239–256 (1998)

(7) K. Yoshida, H. Takami, and N. Shigemi: "Repulsive-Mode Levitation and Propulsion Control of a Land Travelling Marine-Express Model Train ME03", *Proc. of LDIA'95 Nagasaki*, pp.41–44 (1995-6)

(8) K. Yoshida, L. Shi, and T. Yoshida: "A Proposal of Decoupled-Control of Attractive-Normal and Thrust Forces in a SLIM for Maglev Vehicle", *Proc. of the 6th International Conference ELECTRIMACS*, pp.221–226 (1999-9)

(9) K. Yoshida, T. Yoshida, K. Hayashi, and H. Takami: "Decoupled Control of Levitation and Propulsion in SLIM Experimental Maglev Vehicle", *Proc. of ICEM*, Vol.1, pp.228–232 (2000-8)

(10) K. Yoshida, T. Yoshida, and K. Hayashi: "Combined Levitation and Propulsion Control in a SLIM Experimental Maglev Vehicle", *Proc. of 6th ISMST*, Vol.1, pp.404–409 (2001-10)

(11) K. Yoshida and S. Nonaka: "Levitation Forces in Single-Sided Linear Induction Motors for High-speed Ground Transport", *IEEE Trans. on Magn.*, **MAG-11**, No.6, pp.1717–1719 (1975-11)

Kinjiro Yoshida (Member) received the B.S. and M.S. Degrees in Electrical Engineering and Dr. Engineering Degree from Kyushu University, in 1966, 1968 and 1974, respectively. He was an Associate Professor of Dept. of Electrical Engineering at Kyushu University in 1974 and a Professor in 1987. Since April 1996 he has been a Professor of Dept. of Electrical and Electronic Systems Engineering at Kyushu University. From May 1982 to October 1983 he was a Research Fellow of Alexander von Humboldt in TU Braunschweig in West Germany. He is very interested in a new unified theory and application of permanent-magnet and superconducting LSM and LIM for three-dimensionally controlled Maglev systems, especially combined propulsion, levitation and guidance LSM Maglev train, Marine-Express running on both land and underwater and rocket system.

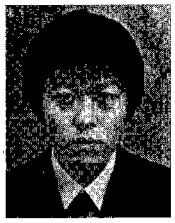

Takashi Yoshida (Student Member) received the B.S. and M.S. Degrees in Electrical Engineering from Kyushu University in 1998 and 2000 respectively. He is now in the Doctor course of the Graduate School of Information Science and Electrical Engineering. He is very interested in drives of LIM and is engaged in the simulation and experiments of LIM vehicle system.